A Free Energy Model for Thin-film Shape Memory Alloys

Jordan E. Massad[*1], Ralph C. Smith[1] and Greg P. Carman[2]

[1] Center for Research in Scientific Computation, N.C. State Univ., Raleigh, NC 27695
[2] Mechanical & Aerospace Engineering Dept., UCLA, Los Angeles, CA 90095

ABSTRACT

Thin-film shape memory alloys (SMAs) have become excellent candidates for microactuator fabrication in MEMS. We develop a material model based on a combination of free energy principles in combination with stochastic homogenization techniques. In the first step of the development, we construct free energies and develop phase fraction and thermal evolution laws for homogeneous, single-crystal SMAs. Second, we extend the single-crystal model to accommodate material inhomogeneities and polycrystalline compounds. The combined model predicts rate-dependent, uniaxial SMA deformations due to applied stress and temperature. Moreover, the model admits a low-order formulation that is suitable for subsequent control design. We illustrate aspects of the model through comparison with thin-film NiTi superelastic hysteresis data.

Keywords: Shape memory alloy model; thin film; superelasticity; activation energy; polycrystalline compounds.

1. INTRODUCTION

In the last 20 years, shape memory alloys (SMAs) have been implemented in a number of high performance applications requiring high work densities, large recoverable deformations, and high stresses. More recently, shape memory alloys have become excellent candidates for microactuators when fabricated as thin films. Their work output density ($\sim$50 MJ m^{-3}) exceeds that of other microactuator mechanisms and they can yield large strokes ($\sim$5%) and forces ($\sim$30 mN). Moreover, thin-film SMAs heat on the order of milliseconds by low voltage ($\sim$5 V) Joule heating, and, unlike bulk SMAs (wires, beams, etc.), their small mass and large surface-to-volume ratio allow fast cooling, potentially permitting switching frequencies on the order of 100 Hz [7].

Current microscale SMA applications include microgrippers [18], micropumps [29], and microcantilever switches [16, 22]. Most of these applications rely on the one-way memory effect and require a biasing mechanism for full actuation. However, microdevices using functionally graded films can achieve two-way, out-of-plane displacement with a smaller footprint than conventional micromechanisms [11, 12]. Superelastic NiTi thin films are being considered for high-strength surface coatings in MEMS devices, and they have potential for microscale mechanical energy storage devices, and vibration dampeners in microelectronics packaging [13, 14]. The reader is referred to [19] for a review of other thin-film SMA applications.

A effort to develop thin-film SMA material models is warranted to ensure the existence of appropriate modeling and simulation tools needed to support design, performance evaluation, and quantification of material capabilities. Models of bulk SMAs capable of accommodating nonlinear material behavior pertinent to actuator design are available. We refer the reader to reviews of a number of bulk SMA models in [4, 5, 6, 10, 25, 26]. In conjunction with advancing fabrication and film characterization technologies, initial thin-film SMA models have been developed [2, 9, 17, 20]. Established bulk models may be considered for thin-film SMAs, provided modifications are made to address issues of scale and the microfabrication process [24].

Focusing on thin-film SMA applications, we employ as a starting point, the Müller-Achenbach-Seelecke theory [1, 23, 27], based on the quantification of thermally activated processes for bulk SMAs. In the first step, we establish local free energies for single-crystal, homogeneous SMAs using Boltzmann statistics to derive rate laws for phase fraction evolution. In addition, we formulate a balance of internal energy that quantifies a rate-dependent release of latent heats and heat transfer to and from the environment. In the second step of the development, we extend the single-crystal model to accommodate inhomogeneous and polycrystalline

---

[*]Corresponding author; Email: jemassad@unity.ncsu.edu; Telephone: 919-515-3745.

materials by considering material parameters to be manifestations of underlying stochastic densities. The result is a rate-dependent, thermomechanical model that predicts relative elongation due to applied stress and temperature. The model accommodates SMA behavior pertinent to actuator design such as superelasticity and the shape memory effect. Moreover, the model admits a low-order formulation suitable for subsequent control design, and most of the model parameters are identifiable directly from standard measurements. In Section 2, we develop the homogeneous SMA model and we extend the model to accommodate nonhomogeneous and polycrystalline SMAs in Section 3. Finally, in Section 4 we validate aspects of the model through comparison with superelastic thin-film SMA data.

2. HOMOGENEOUS MATERIAL MODEL

Motivated by the theory in [27], we treat a lattice layer as the fundamental element of our model. Considering deformations along one axis (across a single habit plane), an SMA lattice layer admits either the austenite phase or one of two martensite variants. We denote the volume fraction of austenite and martensite layers in an SMA as $x_\alpha(t)$, where α represents austenite (A) and martensite $(M^\pm)$. The phase fractions then satisfy the conservation law

$$\sum_\alpha x_\alpha(t) = 1 \tag{1}$$

over all time $t > 0$. Throughout, we assume the martensite variants share the same thermomechanical properties, which generally differ from those of austenite. Once we construct a thermoelastic free energy relation for SMAs, we will model the evolution of the phase fractions due to external stresses and temperatures.

2.1. Free Energy

For a scalar strain ε, we consider the potential for the martensite variants

$$\phi_\pm(\varepsilon, T) = \frac{E_M}{2}(\varepsilon \mp \varepsilon_T)^2 + \beta_M(T), \tag{2}$$

while for austenite we consider

$$\phi_A(\varepsilon, T) = \frac{E_A}{2}\varepsilon^2 + \beta_A(T). \tag{3}$$

The strain-dependent portions of the potentials represent the elastic energies, where the constants E_M and E_A are the linear elastic moduli for martensite and austenite, respectively. The quantity ε_T corresponds to the stress-free equilibrium strain of martensite, while $\varepsilon = 0$ (no deformation) is the equilibrium strain for austenite. The parameter-dependent family of functions

$$\beta_\alpha(T) = c_\alpha(T - T_R) + u_\alpha - Ts_\alpha \tag{4}$$

represent the chemical (non-elastic) free energies [9, 20, 27]. In (4), u_α denote internal energy constants and c_α are phase-dependent specific heat capacities (constant volume) multiplied by the material density. The s_α are specific entropies of the form

$$s_\alpha = c_\alpha \ln\left(\frac{T}{T_R}\right) + \eta_\alpha, \tag{5}$$

where η_α are phase-dependent entropy constants. In (4) and (5), T_R is the temperature of the reference state from which energies and entropies are calculated.

While others such as [9, 17, 20] have formulated the specific Helmholtz free energies as a mixture of (2) and (3), we construct a single, $\mathcal{C}^1$-continuous Helmholtz free energy by joining the individual potentials. Specifically,
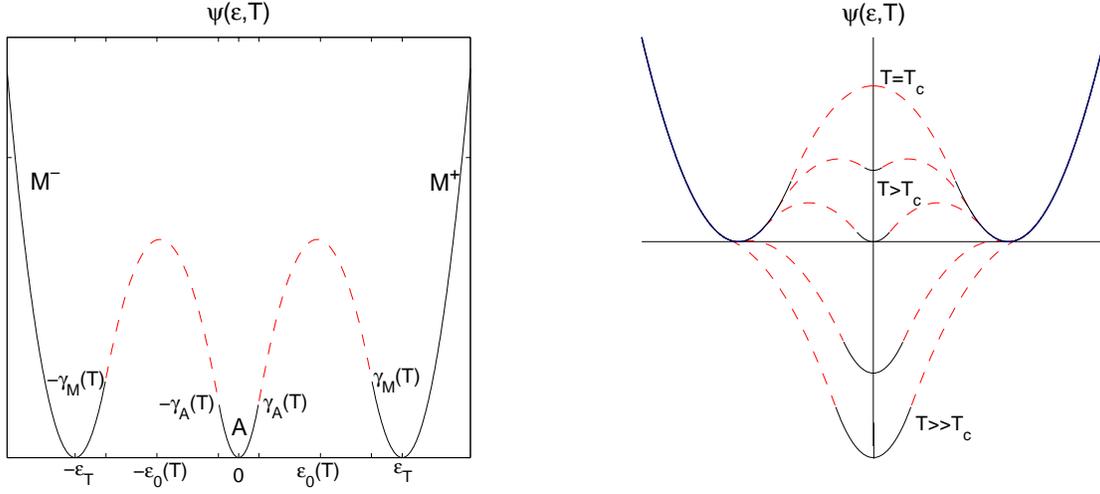
2

Figure 1. Piecewise quadratic Helmholtz free energy density (6) for increasing temperatures; dashed segments represent the concave, unstable states.

we employ the Helmholtz relation

$$\psi(\varepsilon, T) = \begin{cases} \frac{E_M}{2} (\varepsilon + \varepsilon_T)^2 & \varepsilon \leq -\gamma_M(T) \\ -\frac{E_0(T)}{2} (\varepsilon + \varepsilon_0(T))^2 + \psi_0(T) & -\gamma_M(T) < \varepsilon < -\gamma_A(T) \\ \frac{E_A}{2} \varepsilon^2 + \Delta\beta(T) & |\varepsilon| \leq \gamma_A(T) \\ -\frac{E_0(T)}{2} (\varepsilon - \varepsilon_0(T))^2 + \psi_0(T) & \gamma_A(T) < \varepsilon < \gamma_M(T) \\ \frac{E_M}{2} (\varepsilon - \varepsilon_T)^2 & \varepsilon \geq \gamma_M(T) \end{cases}, \tag{6}$$

where $\gamma_M(T)$ and $\gamma_A(T)$ are temperature-dependent nodes connecting the concave parabolae, which represent unstable states, to the convex potentials, which represent stable martensite and austenite states. To facilitate subsequent calculations, we have shifted the martensite minima to zero so that the austenite minimum has height

$$\Delta\beta(T) = \beta_A(T) - \beta_M(T). \tag{7}$$

The temperature-dependent coefficients E_0, ε_0, and ψ_0 define the concave parabolae whose maxima are ψ_0 at $\varepsilon = \pm\varepsilon_0$. Enforcing continuity at the nodes yields

$$-E_A\gamma_A(T)\gamma_M(T) - E_M(\gamma_M(T) - \varepsilon_T)(\varepsilon_T - \gamma_A(T)) = 2\Delta\beta(T), \tag{8}$$

which implicitly provides a thermodynamics-based relation for the nodes via (4) and (7).

Note that the local three-well energy (6) is only valid at temperatures where austenite is stable. We define a local critical temperature T_c below which the austenite phase is unstable upon cooling. Then, (6) holds only for $T > T_c$. At the critical temperature, the austenite nodes converge to $\gamma_A(T_c) = 0$, thereby eliminating the austenite potential well for all lower temperatures. The Helmholtz free energy reduces to a double-well potential for $T \leq T_c$. In this paper, we focus on model development for the three-well potential. Figure 1 illustrates (6) for the full range of temperatures under the assumption $\frac{\partial \Delta\beta}{\partial T} = s_M - s_A < 0$.

The Gibbs free energy density associated with the Helmholtz free energy is

$$G(\varepsilon, \sigma, T) = \psi(\varepsilon, T) - \sigma\varepsilon, \tag{9}$$
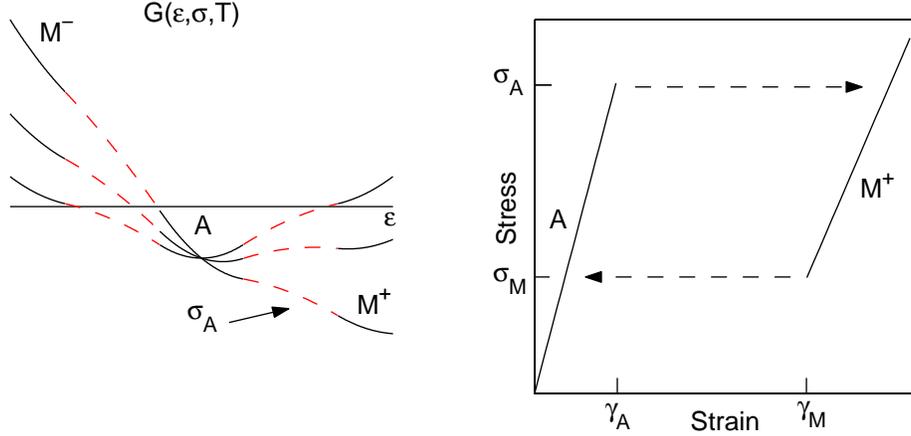
3

Figure 2. The specific Gibbs free energy (9) at a fixed temperature and varying stress. The equilibrium conditions (10) yield a hysteretic stress-strain relation with jumps at the nodes.

where σ is the stress conjugate to ε. Given a stress σ at temperature T, stable equilibrium strains must satisfy

$$\frac{\partial G}{\partial \varepsilon} = 0 \text{ and } \frac{\partial^2 G}{\partial \varepsilon^2} > 0. \tag{10}$$

Given the quadratic form of the local elastic energy, the equilibrium stress-strain relationship yields a linear Hooke's law with hysteresis, as illustrated in Figure 2. The strain values at which jumps occur coincide with the nodes $\pm\gamma_M(T)$ and $\pm\gamma_A(T)$, since they are also inflection points of the Helmholtz energy. We define

$$\sigma_A(T) = E_A \gamma_A(T) \tag{11}$$

and

$$\sigma_M(T) = E_M(\gamma_M(T) - \varepsilon_T), \tag{12}$$

corresponding to the stress values at the jumps. As in [27], we assume the local relation

$$\sigma_A(T) - \sigma_M(T) = \delta, \tag{13}$$

where δ is a material dependent constant estimated from hysteresis data. By the construction of the Gibbs potential, $\sigma_A(T) > \sigma_M(T)$ for all T, so $\delta > 0$. With (11) and (12), we use (13) to formulate (8) in terms of a single temperature-dependent stress (or strain). For example,

$$\Delta\beta(T) = \frac{\delta\varepsilon_T}{2} - \sigma_A(T) \frac{2E_M\delta\varepsilon_T - (1 - E_r)[\delta + \sigma_A(T)]}{2E_M}, \tag{14}$$

where $E_r = E_M/E_A$ is less than one for shape memory compounds. Note that, since $\sigma_A(T_c) = 0$, (14) provides an implicit expression for the critical temperature solely in terms of material constants.

The first order Taylor expansion of (7) about $T = T_R$ is

$$\Delta\beta(T) = \Delta u - \Delta\eta T \tag{15}$$

with truncation error $\mathcal{O}\left((T - T_R)^2\right)$, where $\Delta u = u_A - u_M$ and $\Delta\eta = \eta_A - \eta_M$. Note that (15) is an *exact* relation when $T = T_R$ and for materials in which $\Delta c = c_A - c_M = 0$. Using (14) and (15), we get an *explicit* expression for T_c:

$$T_c = \frac{\Delta u}{\Delta\eta} - \frac{\delta\varepsilon_T}{2\Delta\eta}. \tag{16}$$

4

In an SMA, individual austenite layers become unstable upon cooling at temperatures between the measured martensite start M_s and martensite finish M_f transformation temperatures. Therefore, we estimate T_c for a layer using the relation

$$T_c = \frac{M_s + M_f}{2}. \tag{17}$$

With measurements of transformation temperatures and a transformation stress (e.g., obtained via a tensile test), we use (14) and (17) to calculate the chemical free energy constants Δu and $\Delta \eta$ for an alloy. For example,

$$\Delta \eta = \frac{[2E_M \varepsilon_T - (1 - E_r) \delta] \sigma_h + (1 - E_r) \sigma_h^2}{2E_M (T_h - T_c)} \tag{18}$$

$$\Delta u = \Delta \eta T_c + \frac{\delta \varepsilon_T}{2}, \tag{19}$$

where $T_h > T_c$ is the temperature at which loading transformation stress $\sigma_h = \sigma_A (T_h)$ is measured. A similar approach for identifying the energy constants is employed in [20]. Ultimately, we are able to define the Gibbs potential completely from material data.

2.2. Phase Evolution

Based on the local free energy, we follow the approach in [27] and model the phase evolution with the rate laws

$$\begin{aligned}
\dot{x}_- (t) &= P_{A-} x_A (t) - P_- x_- (t) \\
\dot{x}_A (t) &= P_- x_- (t) - P_{A-} x_A (t) + P_+ x_+ (t) - P_{A+} x_A (t) \\
\dot{x}_+ (t) &= P_{A+} x_A (t) - P_+ x_+ (t),
\end{aligned} \tag{20}$$

where $\cdot$ denotes differentiation in time. The functions $P_\pm$ denote the likelihoods that $M^\pm$ lattice elements will undergo a transformation (to either austenite or a martensite variant), while $P_{A\pm}$ denote the likelihoods that austenite will transform to $M^\pm$. Using the conservation relation (1), the rate law reduces to the two coupled ODEs

$$\begin{aligned}
\dot{x}_- (t) &= - (P_- + P_{A-}) x_- (t) - P_{A-} x_+ (t) + P_{A-} \\
\dot{x}_+ (t) &= - (P_+ + P_{A+}) x_+ (t) - P_{A+} x_- (t) + P_{A+}.
\end{aligned} \tag{21}$$

Next, we formulate the likelihood functions used in (21).

2.3. Transformation Likelihoods

We quantify the probability that a layer will attain specific energy G using the Boltzmann relation

$$\mu (G) = Ce^{-GV/k_B T}, \tag{22}$$

where C is a normalization factor chosen to yield a probability of one when integrating $\mu (G)$ over all energy states. In (22), V is the volume of the layer, and k_B is the Boltzmann constant. Using (22), we compute the likelihood of a martensite layer undergoing a transformation.

$$P_\pm (\sigma, T) = \sqrt{\frac{k_B T}{2\pi m V^{2/3}}} \frac{e^{-G(\pm \gamma_M, \sigma, T)V/k_B T}}{\int_{\pm \gamma_M}^{\pm \infty} e^{-G(\gamma, \sigma, T)V/k_B T} d\gamma} \tag{23}$$

given a stress σ and temperature T, where m is the mass of the layer and $G (\pm \gamma_M, \sigma, T)$ is the Gibbs energy (9) at nodes $\pm \gamma_M (T)$. We have set the integration limits for the normalization factor to cover all possible stable (or metastable) martensite equilibrium states, neglecting the unstable states defined by the concave parabolae

5

in (6). The factor in front of the normalized Boltzmann probability represents the frequency of attempts a layer makes to overcome an energy barrier. Naturally, the frequency increases with increasing activation energy, quantified by the product $k_B T$. Likewise, for the likelihood of an austenite layer undergoing a transformation, we have

$$P_{A\pm}(\sigma, T) = \sqrt{\frac{k_B T}{2\pi m V^{2/3}}} \frac{e^{-G(\pm\gamma_A, \sigma, T)V/k_B T}}{\int_{-\gamma_A}^{\gamma_A} e^{-G(\gamma, \sigma, T)V/k_B T} d\gamma}. \tag{24}$$

Using (11), (12), and (14), we simplify the normalization integrals and express the likelihoods in terms of transformation stresses.

$$P_{\pm}(\sigma, T) = \frac{\sqrt{E_r}}{\tau} \frac{e^{-(\sigma_M \mp \sigma)^2/2\omega_M(T)^2}}{\text{erfc}\left[(\sigma_M \mp \sigma)/\sqrt{2}\omega_M(T)\right]} \tag{25}$$

and

$$P_{A\pm}(\sigma, T) = \frac{1}{\tau} \frac{e^{-(\sigma_A \mp \sigma)^2/2\omega_A(T)^2}}{\text{erf}\left[(\sigma_A + \sigma)/\sqrt{2}\omega_A(T)\right] + \text{erf}\left[(\sigma_A - \sigma)/\sqrt{2}\omega_A(T)\right]}, \tag{26}$$

where

$$\text{erf}(x) = \frac{2}{\sqrt{\pi}} \int_0^x e^{-r^2} dr \tag{27}$$

is the standard error function and $\text{erfc}(x) = 1 - \text{erf}(x)$ is its complement. The resulting factor

$$\tau = \pi \sqrt{\frac{m}{E_A V^{1/3}}} \tag{28}$$

has units of seconds and represents a transformation relaxation time. The functions

$$\omega_\alpha(T) = \sqrt{E_\alpha \frac{k_B T}{V}} \tag{29}$$

quantify thermal activation energy densities for martensite and austenite. Both (25) and (26) have qualities similar to those of normal distributions, where the transformation stresses $\sigma_\alpha(T)$ act as means and $\omega_\alpha(T)$ as standard deviations. Increasing activation energy densities (large variances) allow transformations to occur at wider ranges of stress values approaching $\sigma_\alpha(T)$. Diminishing activation energy densities (small variances) only allow transformations to occur at stresses very near $\sigma_\alpha(T)$.

2.4. Thermal Evolution

We describe uniform temperature changes in the material via a simplified balance of internal energy.

$$\bar{c}(t)\dot{T}(t) = -h_c \Omega\left[T - T_E(t)\right] - \sum_\alpha h_\alpha \dot{x}_\alpha + J(t), \tag{30}$$

where $\bar{c}(t) = \sum_\alpha c_\alpha x_\alpha(t)$ represents the average phase-dependent specific heat. The right-hand side of (30) accounts for heat convection to the environment, where h_c is a convection coefficient, Ω is the SMA surface area-to-volume ratio, and $T_E(t)$ is the external temperature. In general, h_c is temperature and geometry dependent. For this paper, we assume h_c is constant and we refer the reader to [3, 7, 24] for discussions of variable h_c pertinent to bulk and thin-film SMAs.

Equation (30) also accounts for rate-dependent heat generation and loss due to phase transformations, where the specific enthalpies h_α have the form

$$h_\alpha = g_\alpha + T s_\alpha. \tag{31}$$

In (31), g_α is a local minimum of (9) and s_α is the specific entropy from (5). Given stress σ at temperature T,

$$g_A = \frac{-\sigma^2}{2E_A} + \Delta\beta(T) \tag{32}$$

$$g_\pm = \frac{-\sigma^2}{2E_M} \mp \sigma\varepsilon_T. \tag{33}$$

6

Since $\sum_\alpha \dot{x}_\alpha(t) \equiv 0$, we have

$$\sum_\alpha h_\alpha \dot{x}_\alpha = (h_- - h_A)\dot{x}_- + (h_+ - h_A)\dot{x}_+, \tag{34}$$

and

$$h_\pm - h_A = \frac{-\sigma^2}{2}\left(\frac{1}{E_M} - \frac{1}{E_A}\right) \mp \sigma\varepsilon_T - \Delta c(T - T_R) - \Delta u. \tag{35}$$

The differences in martensite and austenite specific enthalpies in (35) are referred to as latent heats of transformation.

Lastly, in (30), $J(t)$ incorporates heat generation via resistive Joule heating, where

$$J(t) = \bar{\rho}^e(t)\frac{I^2}{\zeta^2} \tag{36}$$

for the average, phase-dependent electrical resistivity $\bar{\rho}^e(t) = \sum_\alpha \rho_\alpha^e x_\alpha(t)$, the applied electric current I, and the SMA cross sectional area ζ.

2.5. Average Strain

Given the phase fractions and the thermal evolution modeled by (21) and (30), we quantify the physical response to stress and temperature. Boltzmann statistics govern the response of individual martensite and austenite layers. For martensite, the expectation strains are

$$\langle\varepsilon_-\rangle = \int_{-\infty}^{-\gamma_M} \gamma\mu(G(\gamma, \sigma, T))\,d\gamma \tag{37}$$

and

$$\langle\varepsilon_+\rangle = \int_{\gamma_M}^{\infty} \gamma\mu(G(\gamma, \sigma, T))\,d\gamma, \tag{38}$$

where the Boltzmann function $\mu(G)$ from (22) acts as a probability density function. Likewise for austenite, we have

$$\langle\varepsilon_A\rangle = \int_{-\gamma_A}^{\gamma_A} \gamma\mu(G(\gamma, \sigma, T))\,d\gamma. \tag{39}$$

As with the likelihood functions, we have set the integration limits to cover all possible stable martensite equilibrium states, neglecting the unstable states defined by the concave regions in (6). Evaluating the integrals and using (11), (12), and (14) yield

$$\langle\varepsilon_\pm\rangle = \frac{\pm\tau\omega_M(T)}{E_M\sqrt{E_r\pi}}P_\pm(\sigma, T) + \left(\frac{\sigma}{E_M} \pm \varepsilon_T\right) \tag{40}$$

and

$$\langle\varepsilon_A\rangle = \frac{\tau\omega_A(T)}{E_A\sqrt{\pi}}[P_{A-}(\sigma, T) - P_{A+}(\sigma, T)] + \frac{\sigma}{E_A} \tag{41}$$

in terms of the likelihood functions (25) and (26). From (40) and (41), it is apparent that the expectation strains are the equilibrium solutions (10) to the local Gibbs free energy with perturbations whose magnitudes depend on the activation energy. Indeed, in the limit of vanishing activation energy densities $\omega_\alpha(T)$, (40) and (41) converge to the equilibrium solutions.

With the expectation strain of a layer in each phase, we calculate the average local strain as the weighted sum

$$\varepsilon_{mech} = \sum_\alpha x_\alpha\langle\varepsilon_\alpha\rangle. \tag{42}$$

Apart from the strain ε_{mech} attributed to mechanical deformation and phase transformation processes, there are strains due to thermal expansion as the temperature varies over time. We model the thermal strain as

$$\varepsilon_{therm} = \bar{\lambda}\left(t\right)\left(T - T_0\right) \tag{43}$$

for the average, phase-dependent thermal expansion coefficient $\bar{\lambda}\left(t\right) = \sum_{\alpha} \lambda_{\alpha} x_{\alpha}\left(t\right)$, and initial temperature T_0. Therefore, the total average strain of a layer in response to a combination of applied stress, external temperature, and current is

$$\bar{\varepsilon} = \varepsilon_{mech} + \varepsilon_{therm}. \tag{44}$$

Typically, ε_{therm} is negligible compared to ε_{mech} for moderate temperature changes as would be encountered in bulk superelastic applications. However for thin films in MEMS applications, thermal strains can have significant effects on microdevice behavior (e.g., see [16, 22]).

We have modeled the phase fractions and expected strains with free energy expressions that are valid for *local* lattice behavior. Nevertheless, the model does quantify macroscopic strains for homogeneous, single-crystal SMAs in which the bulk lattice exhibits uniform local behavior. In the next section, we extend our uniform lattice model to inhomogeneous compounds, where the local thermomechanical behavior can vary throughout the material.

3. INHOMOGENEOUS MATERIAL MODEL

Most thin-film SMAs are polycrystalline due to the sputter deposition process. Moreover, precipitates and process-induced impurities may pervade the films. In general, polycrystalline and inhomogeneous materials have a nonuniform lattice structure that can yield variations in the local material response as well as a nonuniform stress field. Measurements of macroscopic phenomena, such as stress-strain hysteresis and transformation temperatures, reflect an average of these variations. Accordingly, to account for inhomogeneities, we treat measured quantities, such as ε_T and δ, as manifestations of distributions, rather than fixed values. In this paper, we construct a statistical distribution about δ by considering

$$\varepsilon\left(\sigma, T\right) = \int_0^{\infty} \bar{\varepsilon}\left(\sigma, T; \delta\right) f_1\left(\delta\right) d\delta, \tag{45}$$

where $\bar{\varepsilon}$ is the local strain in (44), and f_1 is a probability density function defined on $[0, \infty)$. Note that variations in the local transition temperature T_c are also accommodated by varying δ via (14) and (16).

To include the effects of a nonuniform stress field associated with an inhomogeneous lattice, we represent the effective stress on a sample as a perturbation about the macroscopic applied stress. In this case, we take

$$\varepsilon\left(\sigma, T\right) = \int_{-\infty}^{\infty} \bar{\varepsilon}\left(\sigma_e, T\right) f_2\left(\sigma - \sigma_e\right) d\sigma_e, \tag{46}$$

where σ_e is the effective stress perturbation and f_2 is a probability density function defined on $(-\infty, \infty)$. In particular, by distributing about the applied stress, we account for polycrystal grains undergoing stress-induced transformations at different stress levels. We note that a trigonometric distributional averaging is proposed in [23] to accommodate stress variations on rotated polycrystal grains. The combination of (45) and the convolution of (46) yields a relation for the total macroscopic response to a time-varying stress and an evolving internal temperature

$$\varepsilon\left(\sigma, T\right) = \int_0^{\infty} \int_{-\infty}^{\infty} \bar{\varepsilon}\left(\sigma - \sigma_e, T; \delta\right) f_1\left(\delta\right) f_2\left(\sigma_e\right) d\sigma_e d\delta. \tag{47}$$

In the next section, we validate the full model (47) with thin-film SMA hysteresis data.

4. MODEL VALIDATION

A NiTi film of 8μm thickness was deposited onto a Si substrate using a dedicated DC magnetron sputtering system built at the UCLA Active Materials Lab [28]. As described in [12], the system has a temperature-controlled target heater used to make functionally graded films. The target was rated 47.0at%Ni, but microprobe (JEOL JXA-8200) tests prior to deposition indicated the target was 48.5at%Ni and the finished polycrystalline film measured 48.8at.%Ni. After the film was peeled from the substrate, it was post-annealed at 500 °C for 120 minutes.

After annealing, the transformation temperatures were measured with a Shimadzu differential scanning calorimeter yielding $A_s = 56$ °C, $A_f = 80$ °C, $M_s = 61$ °C, $M_f = 50$ °C. Tensile specimens having the dimensions 0.1778 cm width and 1.5 cm gauge length were cut from the film. Using an MTS microtensile apparatus, load-controlled ($0.94\ \mathrm{MPa\,s^{-1}}$) tensile tests were performed in a thermal chamber. The martensite modulus $E_M = 14.0$ GPa was measured from an initial tensile test at 25 °C. The results for the full cycle test conducted at 80 °C are plotted in Figure 3. Near-superelasticity is observed with a 0.11% residual strain. The austenite modulus $E_A = 22.4$ GPa was extrapolated from the loading curve, and the measured loading transformation $\sigma_h = 195$ MPa.

From the superelastic curve at 80 °C, we estimated $\varepsilon_T = 0.0233$ by extrapolating a tangent line from the unloading curve and estimated the mean $\delta = 125$ MPa from the hysteresis thickness. We did not measure the specific heats and published values for thin-film SMAs were not available as estimates. As is typical for bulk NiTi, we assume $\Delta c \approx 0$. Therefore, (30) and (35) simplify accordingly, and σ_h, M_s, and M_f are sufficient to estimate (7). We calculated $h_c = 140\ \mathrm{W\,m^{-2}\,K^{-1}}$ from [24], and the surface area-to-volume ratio $\Omega = 2.511 \times 10^5\ \mathrm{m^{-1}}$. We computed a log-normal distribution about δ using a variance of $(27\ \mathrm{MPa})^2$, and we used an effective stress variance of $(5\ \mathrm{MPa})^2$ with a normal distribution. For the average layer volume, we took $V = 5.0 \times 10^{-23}\ \mathrm{m^3}$ and chose a relaxation time $\tau = 1.7$ ms. For the remaining parameters, we used published NiTi values: $\rho = 6450\ \mathrm{kg\,m^{-3}}$, $c_{VA} = c_{VM} = 837.3\ \mathrm{J\,kg^{-1}\,K^{-1}}$, $\lambda_A = 11.0 \times 10^{-6}\ \mathrm{K^{-1}}$, and $\lambda_M = 6.6 \times 10^{-6}\ \mathrm{K^{-1}}$. For alternative approaches to identifying and measuring these parameters, refer to
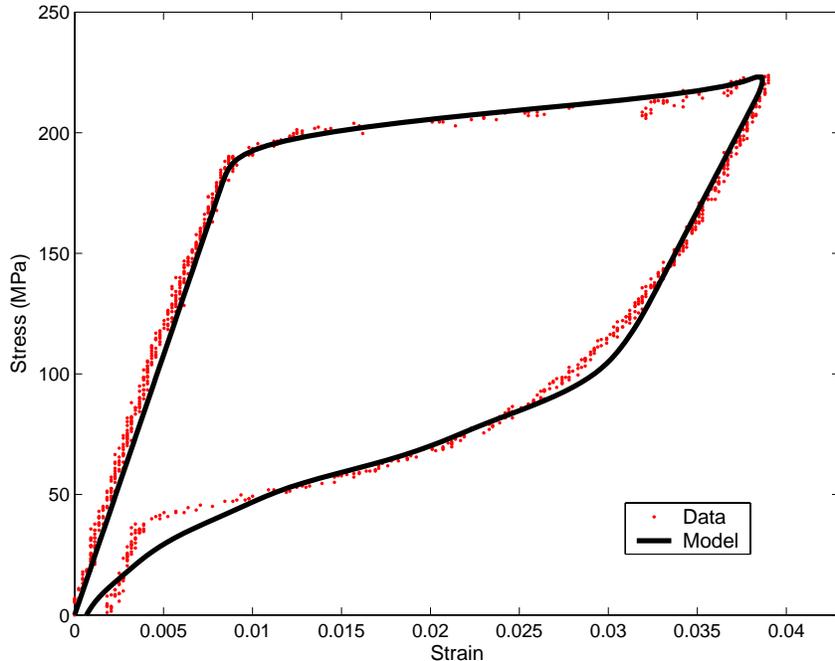

Figure 3: Model fit to thin-film NiTi superelastic hysteresis data.

[3, 8, 21]. The results of the full model with the identified parameters is compared with the data in Figure 3. It is observed that the model accurately predicts the asymmetric loading-unloading curves.

5. CONCLUDING REMARKS

The theory presented here provides a technique for modeling uniaxial hysteresis in SMAs. In the first step of the development, we employ the theory of Müller-Achenbach-Seelecke to develop a local rate-dependent, thermomechanical model applicable to homogeneous single crystals. Then we accommodated inhomogeneous and polycrystalline materials by averaging the variations of local material parameters. The full macroscopic model accurately characterizes superelastic hysteresis of thin-film SMAs as demonstrated in Figure 3. Moreover, the model admits a low-order formulation that is suitable for subsequent control design. Future work includes the development of control algorithms employing robust and multi-objective control frameworks. This will build on previous control analysis for piezoceramic and magnetostrictive materials employed in nonlinear and hysteretic regimes. In addition, after further validation, we will consider integrating the material model into a finite element analysis infrastructure to support future design, performance evaluation, and qualification of thin-film SMA microcomponents.

REFERENCES

1. M. Achenbach, "A model for an alloy with shape memory," *International Journal of Plasticity*, Vol. 5, pp. 371-395, 1989.

2. K. Bhattacharyaa and R.D. James, "A theory of thin films of martensitic materials with applications to microactuators," *Journal of the Mechanics and Physics of Solids*, Vol. 47, pp. 531-576, 1999.

3. A. Bhattacharyya, L. Sweeney and M.G. Faulkner, "Experimental characterization of free convection during thermal phase transformations in shape memory alloy wires," *Smart Materials and Structures*, **11**(3), pp. 411-422, 2002.

4. L.C. Brinson and M.S. Huang, "Simplifications and comparisons of shape memory alloy constitutive models," *Journal of Intelligent Material Systems and Structures*, Vol. 7, pp. 108-114, 1996.

5. B. Bundara, "SMA: Present state and perspective for new applications," *Materials Science Forum*, Vols. 327-328, pp. 43-46, 2000.

6. F. Falk, "Constitutive theories of shape memory alloys related to microstructure," *Proceedings of the SPIE*, Vol. 2442, pp. 2-10, 1995.

7. J.E. Favelukis, A.S. Lavine and G.P. Carman, "An experimentally validated thermal model of thin-film NiTi," *Smart structures and materials 1999: Smart Structures and Integrated Systems, Proceedings of the SPIE*, Vol. 3668, pt. 1-2, pp. 617-629, 1999.

8. Y. Fu, W. Huang, et. al. "Characterization of TiNi shape-memory alloy thin films for MEMS applications," *Surface and Coatings Technology*, **145**(1-3), pp. 107-112, 2001.

9. B. Gabry, C. Lexcellent, et. al., "Thermodynamic modeling of the recovery strains of sputter-deposited shape memory alloys Ti–Ni and Ti–Ni–Cu thin films," *Thin Solid Films*, **372**(1-2), pp. 118-133, 2000.

10. K. Gall, H. Sehitoglu and Y. Chumlakov, "NiTi experiments versus modeling: Where do we stand?" *Smart Structures and Materials 2000: Active Materials: Behavior and Mechanics, Proceedings of the SPIE*, Vol. 3992, pp. 536-547, 2000.

11. J. Gill, D. Chang, et. al., "Manufacturing issues of thin film NiTi microwrapper," *Sensors and Actuators A*, Vol. 93, pp. 148–156, 2001.

12. J. Gill, K. Ho and G.P. Carman, "Three-dimensional thin-film shape memory alloy microactuator with two-way effect," *Journal of Microelectromechanical Systems*, **11**(1), pp. 68-77, 2*002*.

13. D.S. Grummon, S. Nam and L. Chang, "Effect of superelastically deforming NiTi surface microalloys on fatigue crack nucleation in copper," *Shape Memory Materials and Phenomena Fundamental Aspects and Applications Symposium*, pp. 259-264, 1992.

14. L. Hou and D.S. Grummon, "Transformational superelasticity in sputtered titanium-nickel thin films," *Scripta Metallurgica*, Vol. **33**(6), pp. 989-995, 1995.

15. A. Ishida and V. Martynov, "Sputter-deposited shape-memory alloy thin films: properties and applications," *MRS-Bulletin*, **27**(2), pp. 111-114, 2002.

16. A. Ishida, M. Sato, et. al., "Bimorph-type microactuator using TiNi shape-memory film," *Materials Science Forum*, Vols. 394-395, pp. 487-490, 2002.

17. Y.M. Jin and G.J. Weng, "Micromechanics study of thermomechanical characteristics of polycrystal shape-memory alloy films," *Thin Solid Films*, **376**(1-2), pp. 198-207, 2000.

18. M. Kohl, B. Krevet and E. Just, "SMA microgripper system," *Sensors and Actuators A: Physical*, Vols. 97-98, pp. 646-652, 2002.

19. P. Krulevitch, A.P. Lee, et. al., "Thin film shape memory alloy microactuators," *Journal of Microelectromechanical Systems*, **5**(4), pp. 270-282, 1996.

20. C. Lexcellent, S. Moyne, et. al., "Deformation behaviour associated with the stress-induced martensitic transformation in Ti–Ni thin films and their thermodynamical modelling," *Thin Solid Films*, **324**(1-2), pp. 184-189, 1998.

21. S. Miyazaki and A. Ishida, "Martensitic transformation and shape memory behavior in sputter-deposited TiNi-based thin films," *Materials Science and Engineering A*, Vols. 273–275, pp. 106–133, 1999.

22. K. Mori, H. Li, et. al., "Patterned shape memory alloy films," *Materials Transactions*, **43**(5), pp. 951-955, 2002.

23. N. Papenfuß and S. Seelecke, "Simulation and control of SMA actuators," *Smart structures and materials 1999: Mathematics and control in smart structures, Proceedings of the SPIE*, Vol. 3667, pp. 586-595, 1999.

24. J. Peirs, D. Reynaerts and H. Van-Brussel, "Scale effects and thermal considerations for micro-actuators," *Proceedings, 1998 IEEE International Conference on Robotics and Automation*, Vol. 2, pp. 1516-1521, 1998.

25. H. Prahlad and I. Chopra, "Comparative evaluation of shape memory alloy constitutive models with experimental data," *Journal of Intelligent Material Systems and Structures*, **12**(6), pp. 383-394, 2001.

26. B. Schroeder, C. Boller, et. al., "Comparative assessment of models for describing the constitutive behaviour of shape memory alloys," *Smart materials and structures: proceedings of the 4th European Conference on Smart Structures and Materials in conjunction with the 2nd International Conference on Micromechanics, Intelligent Materials, and Robotics*, pp. 305–312, 1998.

27. S. Seelecke and I. Müller, "Shape memory alloy actuators in smart structures - modeling and simulation," *ASME Applied Mechanics Reviews*, to appear, 2003.

28. J. Woolman, "Effect of atomic composition on the mechanical properties of thin film pseudoelastic nickel titanium," Master's Thesis, Mechanical & Aerospace Engineering Department, Univ. of California/Los Angeles, manuscript in preparation.

29. D. Xu, L. Wang, et. al., "Characteristics and fabrication of NiTi/Si diaphragm micropump," *Sensors and Actuators A: Physical*, **93**(1), pp. 87-92, 2001.